
Computational Biology:

# Critical Hydrogen Bond Formation for Activation of the Angiotensin II Type 1 Receptor


Jérôme Cabana, Brian Holleran, Marie-Ève Beaulieu, Richard Leduc, Emanuel Escher, Gaétan Guillemette and Pierre Lavigne

*J. Biol. Chem. 2013, 288:2593-2604.*
*doi: 10.1074/jbc.M112.395939 originally published online December 7, 2012*

---

THE JOURNAL OF BIOLOGICAL CHEMISTRY VOL. 288, NO. 4, pp. 2593–2604, January 25, 2013


# Critical Hydrogen Bond Formation for Activation of the Angiotensin II Type 1 Receptor*

Received for publication, June 27, 2012, and in revised form, December 5, 2012 Published, JBC Papers in Press, December 7, 2012, DOI 10.1074/jbc.M112.395939

**Jérôme Cabana‡, Brian Holleran‡, Marie-Ève Beaulieu‡, Richard Leduc‡, Emanuel Escher‡1, Gaétan Guillemette‡, and Pierre Lavigne§2**

*From the Departments of ‡Pharmacology and §Biochemistry, Faculty of Medicine and Health Sciences, Institut de Pharmacologie de Sherbrooke, Université de Sherbrooke, Sherbrooke, Quecec J1H 5N4, Canada*

**Background:** The N111G and N111W mutations make the $AT_1$ receptor constitutively active and inactivable, respectively.
**Results:** The orientation and interactions of $D74^{2.50}$ are influenced by the residue at position $111^{3.35}$.
**Conclusion:** H-bond formation between $D74^{2.50}$ and $N46^{1.50}$ is critical for $AT_1$ receptor activation.
**Significance:** This novel molecular switch could be involved in the GPCR activation mechanism as it involves highly conserved residues $D^{2.50}$ and $N^{1.50}$.

**G protein-coupled receptors contain selectively important residues that play central roles in the conformational changes that occur during receptor activation. Asparagine 111 ($N111^{3.35}$) is such a residue within the angiotensin II type 1 ($AT_1$) receptor. Substitution of $N111^{3.35}$ for glycine leads to a constitutively active receptor, whereas substitution for tryptophan leads to an inactivable receptor. Here, we analyzed the $AT_1$ receptor and two mutants (N111G and N111W) by molecular dynamics simulations, which revealed a novel molecular switch involving the strictly conserved residue $D74^{2.50}$. Indeed, $D74^{2.50}$ forms a stable hydrogen bond (H-bond) with the residue in position $111^{3.35}$ in the wild-type and the inactivable receptor. However, in the constitutively active mutant N111G-$AT_1$ receptor, residue D74 is reoriented to form a new H-bond with another strictly conserved residue, $N46^{1.50}$. When expressed in HEK293 cells, the mutant N46G-$AT_1$ receptor was poorly activable, although it retained a high binding affinity. Interestingly, the mutant N46G/N111G-$AT_1$ receptor was also inactivable. Molecular dynamics simulations also revealed the presence of a cluster of hydrophobic residues from transmembrane domains 2, 3, and 7 that appears to stabilize the inactive form of the receptor. Whereas this hydrophobic cluster and the H-bond between $D74^{2.50}$ and $W111^{3.35}$ are more stable in the inactivable N111W-$AT_1$ receptor, the mutant N111W/F77A-$AT_1$ receptor, designed to weaken the hydrophobic core, showed significant agonist-induced signaling. These results support the potential for the formation of an H-bond between residues $D74^{2.50}$ and $N46^{1.50}$ in the activation of the $AT_1$ receptor.**

In recent years, a growing number of crystal structures of various family A G protein-coupled receptors (GPCRs)[3] in complex with either agonists or antagonists have been resolved (1–5). Although the sequence similarity of these receptors is rather low (6), there are a few highly conserved residues in every transmembrane domain (TMD), and the three-dimensional arrangement of the TMDs is highly similar in all available crystal structures. These characteristics coupled with results from studies on conformational changes that occur during activation of different family A GPCRs suggest that they may share common activation mechanisms (7–9).

The angiotensin II type 1 ($AT_1$) receptor and its cognate ligand, the octapeptide hormone angiotensin II (AngII), are part of the renin-angiotensin-aldosterone system responsible for controlling blood pressure and water retention via smooth muscle contraction and ion transport, respectively. The $AT_1$ receptor signaling can also induce steroidogenesis in the adrenal gland, neurosecretion, neuronal activation, cell growth, and proliferation (10).

Structure-activity studies on the $AT_1$ receptor have shown that substituting the asparagine residue in position $111^{3.35}$ (see "Experimental Procedures" for details on the residue numbering scheme) for glycine produces a constitutively active mutant receptor, whereas an inactivable mutant is produced when the asparagine is substituted for tryptophan (11). Asparagine 111 ($N111^{3.35}$) is highly, but not strictly, conserved among the family A GPCRs. Homology models of the $AT_1$ receptor that we generated in previous studies (12, 13) suggested that $N111^{3.35}$ is in close proximity to $D74^{2.50}$, which is strictly conserved, as well as $N295^{7.46}$. An interaction between the residues corresponding to $N111^{3.35}$ and $D74^{2.50}$ is notably present in the crystal structures of the human CXC chemokine receptor type 4 (CXCR4) and the mouse $\mu$- and $\delta$- and human $\kappa$- and nociceptin/orphanin FQ opioid receptors (2–5, 14), whereas an interaction between the residues corresponding to $D74^{2.50}$ and $N295^{7.46}$ is featured in the crystal structures of the four opioid receptors mentioned above. Key mutations have stressed the importance of some residues in $AT_1$ receptor activation. Among them, mutation of $D74^{2.50}$ for asparagine or for gluta-

* This work was supported in part by the Canadian Institutes of Health Research.
[1] Recipient of the J. C. Edwards Chair in Cardiovascular Research.
[2] To whom correspondence should be addressed: Dept. of Biochemistry, Faculty of Medicine and Health Sciences, Inst. de Pharmacologie de Sherbrooke, Université de Sherbrooke, 3001 12th Ave. N., Sherbrooke, Quebec J1H 5N4, Canada. Tel.: 819-346-1110 (ext. 15463); E-mail: Pierre.Lavigne@USherbrooke.ca.
[3] The abbreviations used are: GPCR, G protein-coupled receptor; TMD, transmembrane domain; $AT_1$, angiotensin II type 1; AngII, angiotensin II; CXCR4, CXC chemokine receptor type 4; MD, molecular dynamics; $IP_1$, inositol phosphate; Bpa, *p*-benzoyl-l-phenylalanine; Sar, sarcosine.

mate abolished the activity (15), whereas mutation of N295$^{7.46}$ for serine conferred pseudo-constitutive activity to the AT$_1$ receptor (16). The constitutively active N111G-AT$_1$ receptor has been used to study the mechanism of activation of the AT$_1$ receptor using a variety of approaches (12, 13, 17–23, 25–35). These methods have highlighted differences between the AT$_1$ receptor and the N111G-AT$_1$ receptor regarding the solvent-accessible residues delimiting the binding pocket and the ligand contact points. Unlike the AT$_1$ receptor, the constitutively active N111G-AT$_1$ receptor maintains a high affinity conformation despite being uncoupled from its cognate G protein $G_{q/11}\alpha$, whereas the non-activable N111W-AT$_1$ receptor does not couple to $G_{q/11}\alpha$ (11). These results clearly suggest that residue 111 significantly influences the conformational states of the AT$_1$ receptor, but its role at the molecular level is unclear. We hypothesized that residue N111 is part of an interaction network including residues D74$^{2.50}$ and N295$^{2.49}$ that stabilizes an inactive state of the AT$_1$ receptor. To investigate this hypothesis, we used molecular dynamics (MD) simulations of the AT$_1$ receptor (WT, N111G, and N111W) in a solvated lipid bilayer. The simulations revealed H-bond networks that appear specific to the inactive and the active states of the receptor, and they suggest conformational changes required for receptor activation. These simulations have been validated by mutagenesis and *in cellulo* functional assays. The results highlight the importance of the H-bond formed between residues D74$^{2.50}$ and N46$^{1.50}$ in the activation process of the AT$_1$ receptor.

## EXPERIMENTAL PROCEDURES

*Materials*—The two computers used to run the simulations have an Intel Core-i7 quad core processor at 2.67 and 2.93 GHz with 12 and 8 GB of RAM, respectively. All reagents were from Sigma-Aldrich unless otherwise indicated. Culture media, trypsin, FBS, penicillin, and streptomycin were from Wisent (St-Bruno, Quebec, Canada). Opti-MEM was from Invitrogen. Polyethyleneimine was from Polysciences (Warrington, PA). The cDNA clone for the human AT$_1$ receptor was kindly provided by Dr. Sylvain Meloche (University of Montréal). $^{125}$I-[Sar$^1$,Ile$^8$]AngII (specific radioactivity, ~1000 Ci/mmol) was prepared with Iodo-GEN® (Perbio Science, Erembodegem, Belgium) as reported previously (36).

*Residue Numbering Scheme*—Residues of the AT$_1$ receptor are given two numbering schemes. First, residues are numbered according to their positions in the AT$_1$ receptor sequence. Second, residues are also indexed according to their position relative to the most conserved residue in the TMD in which they are located. By definition, the most conserved residue is assigned the position index "50"; *e.g.* in TMD2, D74 is the most conserved residue and was designated D74$^{2.50}$, whereas the upstream residue is designated A73$^{2.49}$, and the downstream residue is designated L75$^{2.51}$. This indexing simplifies the identification of aligned residues in different GPCRs (37).

*Homology Modeling*—We used the I-TASSER server to generate multiple template homology structures of the AT$_1$ receptor. The primary structure of the AT$_1$ receptor used for the modeling can be seen in Fig. 1. The resulting five best structures provided in the output had near identical orientations of the side chains of the H-bond network. We selected the only structure that featured both known disulfides bonds, which had a high confidence score of 0.99 (38, 39). The backbone of the model is very similar to the crystal structure of the CXCR4 receptor (Protein Data Bank code 3ODU) with a root-mean-square deviation distance of 0.900 Å between the positions of C$\alpha$ atoms. Superposition of the two structures is shown in Fig. 2, and sequence alignment between AT$_1$ and CXCR4 is shown in Table 1. The homology model was also analyzed with PROCHECK (40), and the Ramachandran plot indicated that over 97% of the residues were in the "most favored" and "additional allowed" regions. The rest of the stereochemistry was also of high quality. The unstructured N-terminal and C-terminal portions of the model were truncated by removing residues 1–14 and 319–359, respectively, to keep the simulation box as small as possible. This enables better performances for the MD simulations. Models of the N111G-AT$_1$ receptor and N111W-AT$_1$ receptor were generated by replacing residue N111 by the corresponding residue using the mutagenesis feature in PyMOL.

*Molecular Dynamics Simulations*—The GROMACS software suite (41–44) was used to prepare and run the simulations. The AT$_1$ receptor, N111G-AT$_1$ receptor, and N111W-AT$_1$ receptor models were inserted in a lipid bilayer consisting of 128 molecules of dioleoylphosphatidylcholine using the InflateGRO approach (45). Simulation parameters were based on previous work (46–48). The membrane-receptor system was solvated with the simple point charge water model (49). Counterions were added at random positions, replacing water molecules, to keep the net charge of the system at 0. The ffg53a6 force field, modified to use the Berger lipid parameter (50), was used for the calculations. Parameters for the dioleoylphosphatidylcholine molecules and the Protein Data Bank file of the bilayer, developed by Tieleman and co-workers (51–53), were obtained from Peter Tieleman. Equilibration of the system in conditions of constant number of atoms, volume and temperature was performed for 100 ps to reach the desired 310 K temperature. This was followed by equilibration in conditions of constant number of atoms, pressure and temperature for 15 ns with the pressure set at 1 bar. Such long equilibration is necessary for proper equilibration of the lipids after embedding a protein in the membrane (54). We monitored the size of the system in the *x*, *y*, and *z* axes to confirm the stabilization on the dioleoylphosphatidylcholine bilayer. The position of all heavy atoms of the receptor was restrained during equilibration. System size after equilibration in conditions of constant number of atoms, pressure and temperature was $\sim 72 \times 71 \times 79$ Å, ensuring that the AT$_1$ receptor molecule could not interact with its periodic image. Unrestrained MD simulations were run for 84 ns in 2-fs steps. The 84-ns simulation length was deemed long enough for our study, which aimed to analyze side chain reorientation in the core of the AT$_1$ receptor and, to a certain extent, local backbone rearrangements caused by mutations. These motions occur on the nanosecond time scale (55). The simulations were run in periodic boundary conditions at constant temperature (310 K) and pressure (1 bar) using the Nose-Hoover thermostat (56, 57) with $\tau_T = 0.2$ ps and the Parrinello-Rahman barostat with $\tau_P = 5$ ps, respectively. Simulation data were saved every 2 ps for a total of 41,001 frames. Stability of the systems was assessed by calculating the root-mean-square devi-

**TABLE 1**

**Sequence alignment of the AT$_1$ receptor, CXCR4 receptor, κ-opioid receptor, and nociceptin/orphanin FQ receptor**

Sequence alignment was performed by the I-TASSER server. Residues in red represent the most conserved residues within each transmembrane domain. Residues in blue represent other important residues discussed in the text. Numbers represent the Ballestcros numbering of the residue aligned under the last number. Sequences for the CXCR4, κ-opioid receptor (KOR), and nociceptin/orphanin FQ (N/OFQ) receptors are truncated and represent the actual sequences found in the crystal structures of those receptors.

| | |
|---|---|
| | 1.50 2.50 |
| AT1 | MILNSSTEDGIKRIQDDCPKAGRHNYIFVMIPTLYSIIFVVGIFGNSLVVIVIYFYMKLKTVASVFLLNLALADLCFLLTLP |
| CXCR4 | ----------PCFREENANFNKIFLPTIYSIIFLTGIVGNGLVILVMGYQKKLRSMTDKYRLHLSVADLLFVITLP |
| KOR | ----------SPAIPVIITAVYSVVFVVGLVGNSLVMFVIIRYTKMKTATNIYIFNLALADALVTTTMP |
| N/OFQ | ----------PLGLKVTIVGLYLAVCVGGLLGNCLVMYVILRHTKMKTATNIYIFNLALADTLVLLTLP |
| | 3.35 3.50 4.50 |
| AT1 | LWAVYTAMEYRWPFGNYLCKIASASVSFNLYASVFLLTCLSIDRYLAIVHPMKSRLRRTMLVAKVTCIIIWLLAGLASLPAI |
| CXCR4 | FWAVDAVA--NWYFGNFLCKAVHVIYTVNLYSSVWILAFISLDRYLAIVHATNSQRPRKLLAEKVVYVGVWIPALLLTIPDF |
| KOR | FQSTVYLMN-SWPFGDVLCKIVLSIDYYNMFTSIFTLTMMSVDRYIAVCHPVKALDFRTPLKAKIINICIWLLSSSVGISAI |
| N/OFQ | FQGTDILLG-FWPFGNALCKTVIAIDYYNMFTSTFTLTAMSVDRYVAICHPTSSK-------AQAVNVAIWALASVVGVPVA |
| | 5.50 |
| AT1 | IHRNVFFIENTNITVCAFHYESQNSTLPIGLGLTKNILGFLFPFLIILTSYTLIWKALKKAYEIQKNKPRNDDIFKIIMAIV |
| CXCR4 | IFANVSEAD--DRYICDRFYPN--DLWVVVFQFQHIMVGLILPGIVILSCYCIIISKLSHSGSNISKGHQKRKALKTTVILI |
| KOR | VLGGTKVREDVDVIECSLQFPDDDSWWDLFMKICVFIFAFVIPVLIIIVCYTLMILRLKSVRLLSD--RNLRRITRLVLVVV |
| N/OFQ | IMGSAQVEDEEIE--CLVEIPTPQDYWGPVFAICIFLFSFIVPVLVISVCYSLMIRRLRGVRLLSGSDRNLRRITRLVLVVV |
| | 6.50 7.50 |
| AT1 | LFFFFSWIPHQIFTFLDVLIQLGIIRDCRIADIVDTAMPITICIAYFNNCLNPLFYGFLGKKFKRYFLQLLKYIPPKAKSHS |
| CXCR4 | LAFFACWLPYYIGISIDSFILLEIIQGCEFENTVHKWISITEALAFFHCCLNPILYAFLGAKFKTSAQHALTSGRPLEVLFQ |
| KOR | AVFVVCWTPIHIFILVEALG----------ALSSYYFCIALGYTNSSLNPILYAFLDENFKRCFRDFCFP--------- |
| N/OFQ | AVFVGCWTPVQVFVLAQGLG------VQPSSETAVAILRFCTALGYVNSCLNPILYAFLDENFKACFR---------- |
| | |
| AT1 | NLSTKMSTLSYRPSDNVSSSTKKPAPCFEVE |
| CXCR4 | ---------- |
| KOR | ---------- |
| N/OFQ | ---------- |

ation distance between the positions of Cα atoms of the TMDs during the simulations. In all three instances, the root-mean-square deviations converged to a similar and stable value, close to 2.5Å, indicating that equilibrium was reached before initiating the MD simulation of all three systems.

*Trajectory Analysis*—MD trajectories output from GROMACS were converted to Protein Data Bank files with 211 frames (one for every 200 saved) for visual inspection with PyMOL (58) and to compressed .xtc trajectory files with 2101 frames (one for every 20 saved) for other analyses. Evaluation of the presence of H-bonds during the simulations was performed with the g_hbond tool in GROMACS using the default cutoff angle value of 30° and a cutoff radius of 0.35 nm. Data regarding distances, dihedral angles, water occupancy, and water molecule count were performed with the g_dist, g_angle, g_spatial, and g_mindist tools, respectively, within GROMACS. Statistical analyses were performed using Student's *t* test. Results were considered statistically significant when $p < 0.01$ (*).

*Oligodeoxynucleotide Site-directed Mutagenesis*—Site-directed mutagenesis was performed on the AT$_1$ receptor or relevant mutants using the QuikChange II XL mutagenesis kit (Stratagene, La Jolla, CA) as recommended by the manufacturer. Briefly, forward and reverse oligonucleotides were constructed to introduce the N46G mutation in the AT$_1$ receptor or in the N111G-AT$_1$ receptor background and the F77A mutation in the AT$_1$ receptor or in the N111W-AT$_1$ receptor background. Site-directed mutations were then confirmed by automated DNA sequencing by aligning the AT$_1$ receptor sequence with multiAlin (59).

*Cell Culture and Transfection*—HEK293 cells were maintained in DMEM supplemented with 10% FBS, 100 IU/ml penicillin, and 100 μg/ml streptomycin at 37 °C in a humidified 5% $CO_2$ atmosphere. The day prior to transfection, cultured cells were washed with phosphate-buffered saline (PBS) at room temperature, trypsinized, and seeded at 150,000 cells/well in a 6-well plate. For transfection, 2 μg of the DNA construct containing the appropriate AT$_1$ receptor construct was added to 100 μl of Opti-MEM containing 6 μg of polyethyleneimine, and the mixture was incubated for 20 min before being added to the cultured cells as described previously (60).

*Inositol Phosphate Production*—Inositol phosphate (IP$_1$) production was determined using the IP-One assay (Cisbio Bioassays, Bedford, MA). Necessary dilutions of the agonist AngII were prepared in stimulation buffer (10 mM Hepes, 1 mM $CaCl_2$, 0.5 mM $MgCl_2$, 4.2 mM KCl, 146 mM NaCl, 5.5 mM glucose, 50 mM LiCl, pH 7.4). 48 h after transfection, the cells were washed with PBS at room temperature. The cells were trypsinized and distributed at 20,000 cells/well (7 μl) in a white 384-well plate in stimulation buffer. Cells were stimulated at 37 °C for 30 min with increasing concentrations of AngII. Cells were then lysed with 3 μl of IP$_1$ coupled to the dye d2. After addition of 3 μl of anti-IP$_1$ cryptate terbium conjugate, cells were incubated for 1 h at room temperature under agitation. FRET signal was measured with a Tecan M1000 plate reader.

*Binding Experiments*—HEK293 cells were grown for 36 h after transfection in 100-mm culture dishes and subjected to one freeze-thaw cycle. Broken cells were then gently scraped

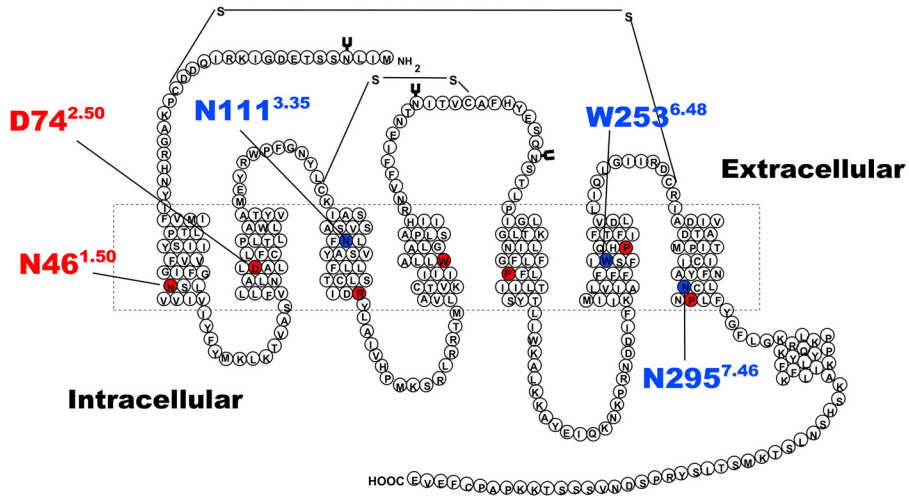


FIGURE 1. **Two-dimensional schematic representation of the primary amino acid structure of the AT$_1$ receptor.** The *dashed rectangle* represents the lipid bilayer where the seven TMD are located. Residues in *red* correspond to the most conserved residue in each TMD that are notably important for sequence alignment during homology modeling procedures. Labeled residues in *red* and residues in *blue* represent important residues discussed in this study.

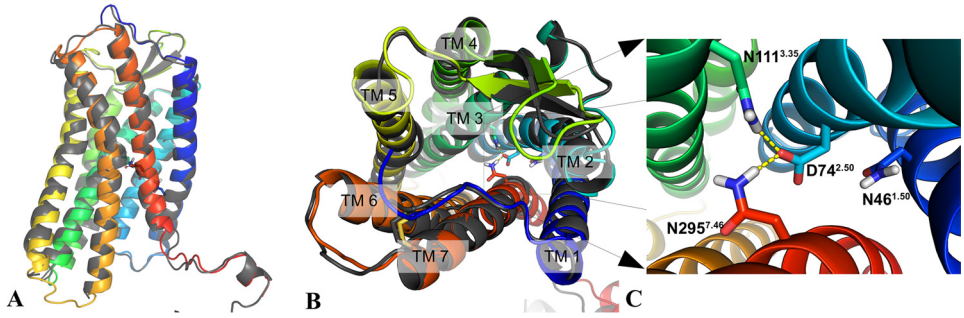


FIGURE 2. **The I-TASSER server was used to produce a homology model of the AT$_1$ receptor.** *A*, the backbone of the AT$_1$ receptor homology model (*colored*) closely matches the backbone of the crystal structure of the CXCR4 receptor (*gray*). The side chains of residues N46$^{1.50}$, D74$^{2.50}$, N111$^{3.35}$, and N295$^{7.46}$ of the AT$_1$ receptor are shown as *sticks* visible through the *semitransparent* backbone representation. *B*, view from the top (from the extracellular side looking toward the intracellular side) of the superposition of the AT$_1$ receptor homology model (*colored*) and the CXCR4 receptor (*gray*). *C*, zoomed-in view showing the H-bonds (*yellow dashes*) formed between N111$^{3.35}$, D74$^{2.50}$, and N295$^{7.46}$ in the AT$_1$ receptor homology model. Hydrogen, nitrogen, and oxygen atoms are shown in *white*, *blue*, and *red*, respectively. Carbon atoms are colored according to the TMD in which they are located.

into washing buffer (25 mM Tris-HCl, pH 7.4, 100 mM NaCl, 5 mM $MgCl_2$), centrifuged at 2500 × *g* for 15 min at 4 °C, and resuspended in binding buffer (25 mM Tris-HCl, pH 7.4, 100 mM NaCl, 5 mM $MgCl_2$, 0.1% bovine serum albumin, 0.01% bacitracin, 0.01% soybean trypsin inhibitor). Saturation binding experiments were done by incubating broken cells (20–40 μg of protein) for 1 h at room temperature with increasing concentrations of $^{125}$I-[Sar$^1$,Ile$^8$]AngII in a final volume of 500 μl. Nonspecific binding was determined in the presence of 1 μM unlabeled [Sar$^1$,Ile$^8$]AngII. Bound radioactivity was separated from free ligand by filtration through GF/C filters presoaked for at least 3 h in binding buffer. Receptor-bound radioactivity was evaluated by γ counting. Results are presented as means ± S.D. Binding data ($B_{max}$ and $K_d$) were analyzed with Prism version 5.0 for Windows (GraphPad Software, San Diego, CA) using a one-site binding hyperbola nonlinear regression analysis. Dose displacement experiments were done by incubating broken cells (20–40 μg of protein) for 1 h at room temperature with 0.8 nM $^{125}$I-[Sar$^1$,Ile$^8$]AngII as tracer and increasing concentrations of AngII. The $K_d$ values in the displacement studies were determined from the $IC_{50}$ values using the Cheng-Prusoff equation (61).

## RESULTS

*Rearrangement of the N111-D74-N295 H-bond Network Caused by the N111G Mutation*—An updated version of the homology model of the AT$_1$ receptor (Fig. 1) that includes the latest structural knowledge has been generated using the I-TASSER server (38, 39) (Fig. 2, *A* and *B*). The backbone structure of the homology model closely matches that of the CXCR4 crystal structure (Protein Data Bank code 3ODU) with a root-mean-square deviation of 0.900 Å between the Cα atoms. In this model, a network of H-bonds involving residues D74$^{2.50}$, N111$^{3.35}$, and N295$^{7.46}$ is revealed (Fig. 2*C*). This network displayed a high stability throughout the 84-ns MD simulation of the AT$_1$ receptor (Fig. 3*A*). More precisely, analysis of the MD simulation indicated that an H-bond was present between the side chain of N111 and those of D74 and N295 64.6 and 56.4% of the time, respectively (data not shown). In addition, an H-bond between the side chains of D74 and N295 was present 98.0% of the time. On the other hand, an H-bond formed 1.4% of the time between the side chains of D74 and N46. Interestingly, the MD simulation showed that within the constitutively active N111G-AT$_1$ receptor the side chain of residue D74$^{2.50}$ reorients toward TMD1 within 1 ns to form an H-bond with the side

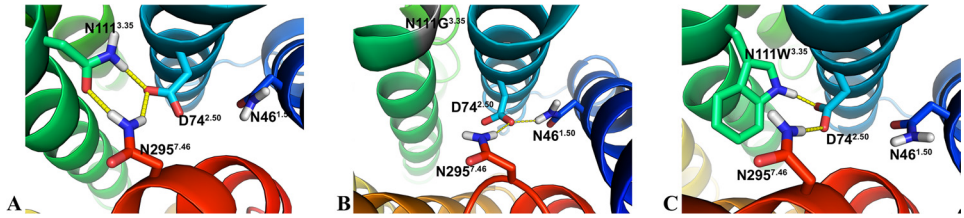


FIGURE 3. **The orientation of D74$^{2.50}$ and the N111-D74-N295 H-bond network are affected by the residue at position 111$^{3.35}$.** *A*, snapshot of the 84-ns MD simulation of the AT$_1$ receptor showing the N111-D74-N295 H-bond network. *B* and *C*, snapshots of the 84-ns MD simulations showing the N46-D74-N295 network in the N111G-AT$_1$ receptor (*B*) and the W111-D74-N295 network in the N111W-AT$_1$ receptor (*C*). H-bonds are shown as *yellow dashed lines*. Hydrogen, nitrogen, and oxygen atoms are shown in *white*, *blue*, and *red*, respectively. Carbon atoms are colored according to the TMD in which they are located.

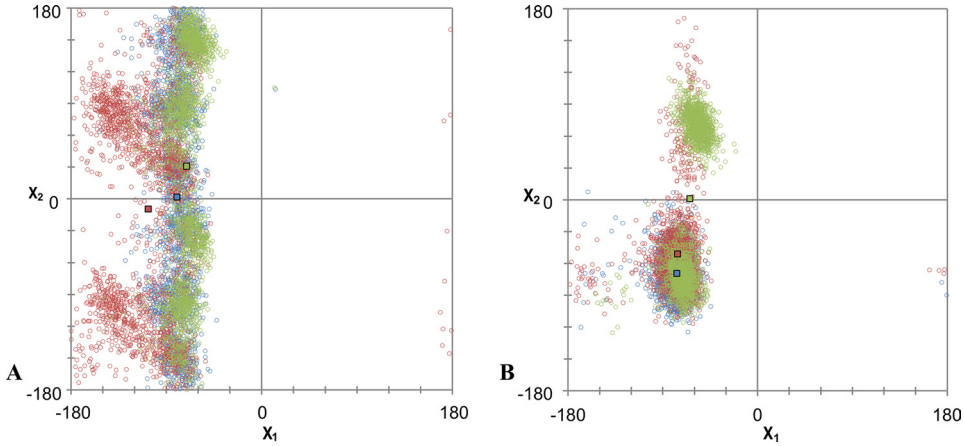


FIGURE 4. **Analysis of the $\chi_1$ and $\chi_2$ angles (*x* and *y* axes, respectively) of the side chain of residue D74$^{2.50}$ (*A*) and N46$^{1.50}$ (*B*) from 2100 frames of the 84-ns MD simulation of the AT$_1$ receptor (*blue*), N111G-AT$_1$ receptor (*red*) and N111W-AT$_1$ receptor (*green*).** *Colored squares* represent the average $\chi_1$ and $\chi_2$ values in each simulation.

chain of N46$^{1.50}$ (Fig. 3*B*). Indeed, analysis of the MD trajectory using g_hbond indicated that the H-bond between the side chains of N46$^{1.50}$ and D74$^{2.50}$ was present 34.1% of the time in the N111G-AT$_1$ receptor. As to the H-bond between the side chains of D74$^{2.50}$ and N295$^{7.46}$, the analysis revealed that it was present 88% of the time in the N111G-AT$_1$ receptor. Analysis of the rotamers of residue D74$^{2.50}$ revealed that $\chi_1$ maintains a *gauche* (−) conformation 99.5% of the time throughout the simulation of the AT$_1$ receptor, whereas in the N111G-AT$_1$ receptor, it explored a *trans* conformation 35.6% of the time (Fig. 4*A*). These results suggest that the N111-D74-N295 H-bond network rearranges to form the new N46-D74-N295 H-bond network in the context of receptor constitutive activity.

*Structural Changes Induced by the N111G Mutation*—The most important conformational change observed in the backbone of the N111G-AT$_1$ receptor mutant was located in TMD7. Indeed, the $\alpha$-helical geometry is distorted in the portion of TMD7 encompassing residues I290$^{7.41}$ to F293$^{7.44}$ during the MD simulation (Fig. 5*A*). The Ramachandran plots for these residues clearly show that the backbone explored conformations in the $\beta$-strand quadrant for A291$^{7.42}$ and Y292$^{7.43}$ (data not shown). The associated increase in pitch for this portion of TMD7 was assessed by measuring the distance between the $\alpha$-carbon atoms of residues C289$^{7.40}$ and N294$^{7.45}$. On average, the distance between these two atoms was 9.1 ± 0.5 Å for the AT$_1$ receptor and 13.2 ± 0.8 Å for the N111G-AT1 receptor (Fig. 5, *B* and *C*).

To identify additional structural differences between the AT$_1$ receptor and the N111G-AT$_1$ receptor, we measured

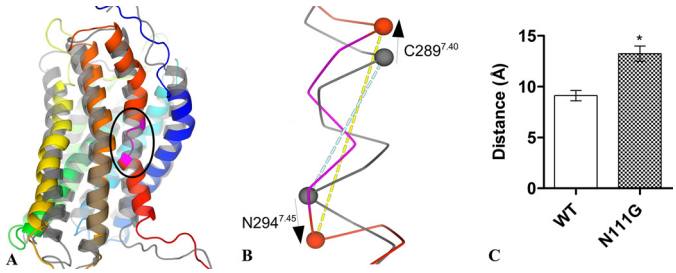


FIGURE 5. **The helicity of TMD7 is disturbed in the N111G-AT$_1$ receptor.** *A*, the final frame of the 84-ns MD simulations of the N111G-AT$_1$ receptor (*colored*) shows that the helicity of TMD7 (*red*) is locally disturbed between residues I290 and F293 (*pink* section shown within *circled* area). The final frame of the 84-ns simulation of the AT$_1$ receptor (*gray*) is superimposed for comparison. *B*, the zoomed-in view of the *circled* area of TMD7 shows the increased distance between the C$\alpha$ atoms of C289$^{7.40}$ and N294$^{7.45}$ (shown as *spheres*). The *blue* and *yellow dashed lines* represent the measured distances between residues C289$^{7.40}$ and N294$^{7.45}$ in the AT$_1$ receptor and N111G-AT$_1$ receptor, respectively. *C*, distance between the $\alpha$-carbon of residues C289$^{7.40}$ and N294$^{7.45}$. Data are the mean ± S.D. (*error bars*) of 2100 frames from each 84-ns MD trajectory. *, significantly different ($p < 0.01$).

the distance between C$\alpha$ atoms of the residues involved in the H-bond networks described above. Over the course of the MD simulations, the average distance between the C$\alpha$ atoms of residues 111$^{3.35}$ and N295$^{7.46}$ increased by 1.7 Å from 9.4 Å in the AT$_1$ receptor to 11.1 Å in the N111G-AT$_1$ receptor (Fig. 6). Interestingly, the average distance between the C$\alpha$ atoms of residues N46$^{1.50}$ and N295$^{7.46}$ decreased by 1.7 Å from 10.1 Å in the AT$_1$ receptor to 8.4 Å in the N111G-AT$_1$ receptor (Fig. 6). Although significant (due to the large number of data), a very minor decrease in the distance between the C$\alpha$ atoms of

D74$^{2.50}$ and N295$^{7.46}$ was observed (6.9 Å in the AT$_1$ receptor and 6.8 Å in the N111G-AT$_1$ receptor) (Fig. 6).

These results suggest that during the process of activation the reorientation of D74$^{2.50}$ is accompanied with a concerted movement of N295$^{7.46}$ away from TMD3 and toward TMD1 that causes a local conformational change of TMD7. We propose that this movement is facilitated by the apparent stability of the H-bond between the side chains of D74$^{2.50}$ and N295$^{7.46}$.

To evaluate the impact of the side chain rearrangement and movement of TMD7 on the water accessibility within the receptor, we used the spatial density function (62) of GROMACS to calculate the water occupancy in the molecular dynamics trajectories of the AT$_1$ receptor and the N111G-AT$_1$ receptor (Fig. 7). A difference was observed in the upper portions of TMD3 and TMD7 (toward the extracellular side) roughly up to two helical turns above N295$^{7.46}$. This area was much more accessible to water molecules within the constitutively active N111G-AT$_1$ receptor (Fig. 7*B*) than within the AT$_1$ receptor (Fig. 7*A*). Interestingly, this area includes the portion of TMD7 that experiences conformational changes in the N111G-AT$_1$ receptor. This area contains a cluster of hydrophobic residues consisting of residues V108$^{3.33}$, L112$^{3.36}$, I288$^{7.39}$, A291$^{7.42}$, Y292$^{7.43}$, and F77$^{2.53}$. The MD simulations suggested that, within the AT$_1$ receptor, these residues form a tight hydrophobic core (Fig. 7*A*), which is disrupted within the N111G-AT$_1$ receptor (Fig. 7*B*). To support the information obtained from the spatial density function, we evaluated the number of water molecules within a 5-Å distance of the cluster of hydrophobic residues. Analysis of the MD trajectories using the GROMACS tool g_mindist revealed that, on average, 16 water molecules were within 5 Å of the hydrophobic cluster in the AT$_1$ receptor, whereas 26 water molecules were within 5 Å of the hydrophobic cluster in the N111G-AT$_1$ receptor (Fig. 8). Interestingly MD trajectories indicate that in the N111G-AT$_1$ receptor water molecules form H-bonds with the backbone carbonyl of I288 and A291, two residues located in the region of TMD7 that has lost its helicity (Fig. 9). This gain in water accessibility within the N111G-AT$_1$ receptor was accompanied by a 3-Å increase in the average distance between TMD3 and TMD7 in the portion of helices containing residues V108$^{3.33}$ to L112$^{3.36}$ and I288$^{7.39}$ to Y292$^{7.43}$ (Fig. 10).

Interestingly, the hydrophobic cluster is adjacent to W253$^{6.48}$, a conserved tryptophan residue that is part of the CW*X*P motif in TMD6 and commonly known as the "rotamer toggle switch" (63, 64). The MD trajectories of the AT$_1$ receptor suggested that W253$^{6.48}$ maintains its hydrophobic indole moiety in an orientation allowing a direct contact with the hydrophobic core, more precisely with residues A291$^{7.42}$ and L112$^{3.36}$ (Fig. 11*A*). Conversely, the MD trajectories of the N111G-AT$_1$ receptor revealed that the indole moiety of W253$^{6.48}$ is oriented away from the hydrophobic cluster toward TMD5 (Fig. 11*B*). These results suggest that the N111G mutation disrupts the hydrophobic cluster and increases the solvent accessibility in that area of the receptor, apparently influencing the orientation of the side chain of W253$^{6.48}$.

*Conserved Residue N46$^{1.50}$ Is Important for AT$_1$ Receptor Activation*—MD simulations suggested that a highly stable N111-D74-N295 H-bond network within the AT$_1$ receptor rearranges to form a new N46-D74-N295 H-bond network within the constitutively active N111G-AT$_1$ receptor. The

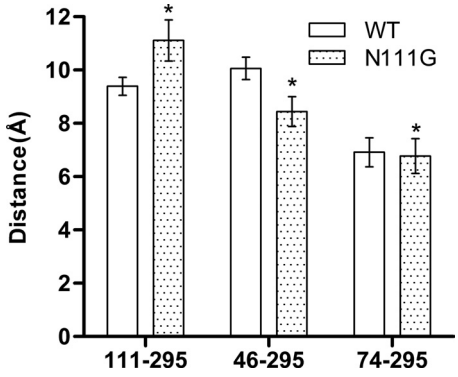


FIGURE 6. **Conformational changes between the AT$_1$ receptor and N111G-AT$_1$ receptors revealed by the analysis of the MD trajectories.** Histograms of the average distance between the C$\alpha$ atoms of residues 111$^{3.35}$ and N295$^{7.46}$, N46$^{1.50}$ and N295$^{7.46}$, and D74$^{2.50}$ and N295$^{7.46}$ are shown. Data are the mean ± S.D. (*error bars*) of 2100 frames from each 84-ns MD trajectory. *, significantly different from AT$_1$ receptor ($p < 0.01$).

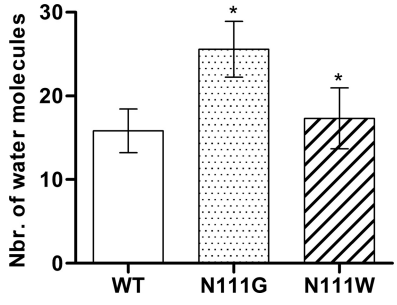


FIGURE 8. **Number of water molecules in the area near the hydrophobic cluster of the AT$_1$ receptor, the N111G-AT$_1$ receptor, and the N111W-AT$_1$ receptor.** Analyses of the 84 ns MD trajectories shows the average number of water molecules within 5Å of residues V108$^{3.33}$, L112$^{3.36}$, I288$^{7.39}$, A291$^{7.42}$, Y292$^{7.43}$ and F77$^{2.53}$. Data are the mean ± S.D. (*error bars*) of 2100 frames from each 84 ns MD trajectory. *, significantly different from AT$_1$ receptor ($p <$ 0.01).

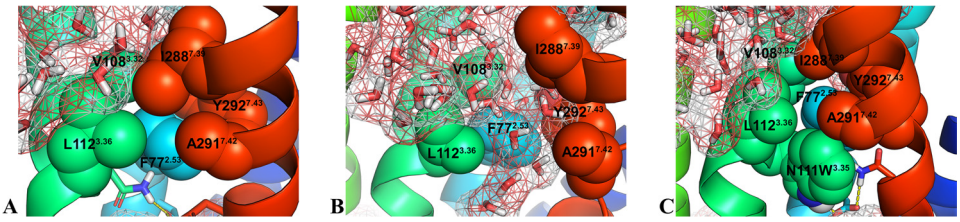


FIGURE 7. **Snapshots of the 84-ns MD simulations showing the water molecules (*red* and *white sticks*; molecular surface in *mesh*) in the area near the hydrophobic cluster between TMD2 (*light blue*), TMD3 (*green*), and TMD7 (*red*).** The hydrophobic residues F77$^{2.53}$ (*light blue*), V108$^{3.33}$ (*green*), L112$^{3.36}$ (*green*), I288$^{7.39}$ (*red*), A291$^{7.42}$ (*red*), and Y292$^{7.43}$ (*red*) are displayed in *spheres*. Water molecules are shown in the AT$_1$ receptor (*A*), the N111G-AT$_1$ receptor (*B*), and the N111W-AT$_1$ receptor.

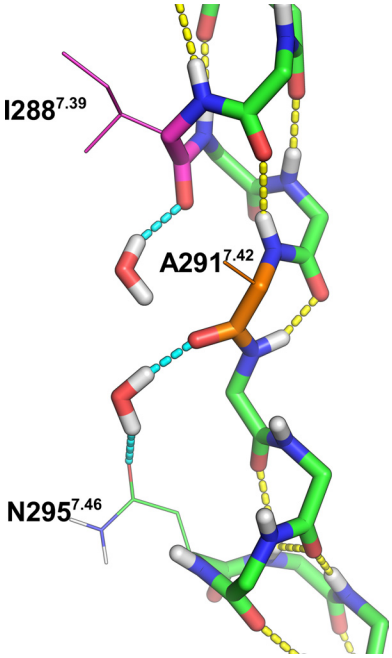


FIGURE 9. **Snapshot of the 84-ns MD trajectory of the N111G-AT$_1$ receptor showing water molecules interacting with backbone atoms of TMD7.** Water molecules and backbone atoms are shown as *sticks*. Side chain atoms are shown as *thin lines*. Hydrogen, nitrogen, and oxygen atoms are shown in *white*, *blue*, and *red*, respectively. Carbon atoms are *green* or as specified. *Yellow dashes* represent intrabackbone H-bonds. *Light blue dashes* represent H-bonds involving water. One water molecule interacts with the backbone carbonyl of I288$^{7.39}$ (*magenta*), and one water molecule interacts with the backbone carbonyl of A291$^{7.42}$ (*orange*) and with the side chain of N295$^{7.46}$.

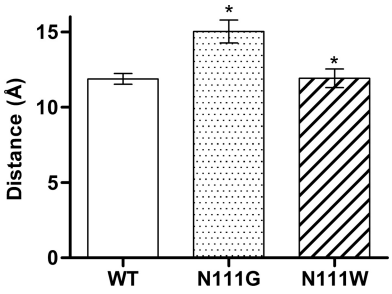


FIGURE 10. **Histograms showing the average distance between the portions of helices (center of mass) containing residues V108$^{3.33}$ to L112$^{3.36}$ on TMD3 and I288$^{7.39}$ to Y292$^{7.43}$ on TMD7.** Data are the mean ± S.D. (*error bars*) of 2100 frames from each 84-ns MD trajectory.*, significantly different from AT$_1$ receptor ($p < 0.01$).

H-bond between D74$^{2.50}$ and N46$^{1.50}$ thus appears to play an important role in receptor activation. To support this possibility, we evaluated the functional properties of mutant receptors in which N46 was substituted for a glycine (N46G-AT$_1$ receptor and N111G/N46G-AT$_1$ receptor) and compared them with the AT$_1$ receptor and the N111G-AT$_1$ receptor. Table 2 shows that all the constructs were efficiently expressed and exhibited high binding affinities. The functional properties of the wild-type and mutant AT$_1$ receptors were evaluated by assessing the basal and AngII-induced production of IP$_1$ in transiently transfected HEK293 cells (Table 3). Fig. 12*A* shows that the basal level of IP$_1$ in cells expressing the constitutively active N111G-AT$_1$ receptor was significantly higher (75.9 ± 4.4 nM) than the basal level of IP$_1$ in cells expressing the AT$_1$ receptor (27.2 ± 8.0 nM). Upon stimulation with increasing concentrations of AngII, the constitutively active receptor increased the IP$_1$ to a maximal level (224.3 ± 5.6 nM) that was not significantly different from that obtained with the AT$_1$ receptor (235.4 ± 7.3 nM). The basal level of IP$_1$ in cells expressing the N111G/N46G-AT$_1$ receptor (9.2 ± 0.7 nM) was not significantly different from the level of IP$_1$ in mock-transfected cells (7.1 ± 0.7 nM). Furthermore, AngII-induced IP$_1$ production in cells expressing the N111G/N46G-AT$_1$ receptor was completely blunted. Fig. 12*A* also shows that the basal level of IP$_1$ in cells expressing the N46G-AT$_1$ receptor was very low (8.2 ± 1.1 nM) and that this level marginally increased (57.5 ± 1.6 nM) upon stimulation with a maximal concentration of AngII. These results indicate that residue N46$^{1.50}$ plays an important role in agonist-induced activation of the AT$_1$ receptor, and it also stabilizes an active state of the AT$_1$ receptor in the absence of any agonist. At the molecular level, the N111G mutation appears to disrupt the interaction between N111$^{3.35}$ and D74$^{2.50}$ that reorients toward N46$^{1.50}$, thus inducing a conformational change responsible for the constitutive activity.

We also verified whether the inactivable D74N-AT$_1$ receptor could be rescued by the N111G mutation. Fig. 12*B* shows that the basal level of IP$_1$ in cells expressing the D74N-AT$_1$ receptor was low (27.8 ± 4.7 nM) and barely increased upon stimulation with AngII (41.6 ± 4.9 nM). In cells expressing the D74N/N111G-AT$_1$ receptor, the basal level was slightly lower compared with cells expressing the N111G-AT$_1$ receptor (45.1 ± 3.8 nM). Stimulation of this mutant receptor with AngII produced only a weak increase in IP$_1$ level (85.8 ± 6.6 nM). The presence of an aspartate at position 74$^{2.50}$ appears to be crucial to the mechanism of activation as substitution of residue D74$^{2.50}$ for an asparagine significantly hampered constitutive and agonist-induced activity of the receptor.

*The H-bond between Residues 111$^{3.35}$ and D74$^{2.50}$ Is Stabilized by the N111W Mutation*—The MD trajectories of the N111W-AT$_1$ receptor showed that an H-bond network involving the side chains of residues W111$^{3.35}$, D74$^{2.50}$, and N295$^{7.46}$ was very stable (Fig. 3*C*). Analysis of the trajectory revealed that an H-bond between the side chains of W111$^{3.35}$ and D74$^{2.50}$ was present 83.6% of the time in this inactivable receptor. The higher apparent stability of this interaction within the N111W-AT$_1$ receptor is likely due to the fact that the H-bond donor of the tryptophan is in the ϵ position and therefore closer to D74$^{2.50}$ than the H-bond donor of the asparagine (which is in δ position), hence leading to a stronger H-bond. To test this assumption, we evaluated the distribution of the length of the H-bonds formed between the side chains of residues W111$^{3.35}$ and D74$^{2.50}$ throughout the simulation. Compared with the H-bond formed between N111$^{3.35}$ and D74$^{2.50}$, the average distance of the H-bond between W111$^{3.35}$ and D74$^{2.50}$ is smaller by 0.04 Å (2.93 *versus* 2.97 Å). More strikingly, this H-bond is shorter than 2.8 Å 27.7% of the time for the N111W-AT$_1$ receptor compared with 16.1% for the AT$_1$ receptor (data not shown). In addition, we observed that an H-bond between the side chains of D74$^{2.50}$ and N295$^{7.46}$ was persistent (95.9% of the time), whereas the side chains of W111$^{3.35}$ and N295$^{7.46}$ made an H-bond only 0.3% of the time. However, the side chains of D74$^{2.50}$ and N46$^{1.50}$ were engaged in an H-bond 18.9% of the time. It is interesting to note that the $\chi_1$ angle of D74$^{2.50}$

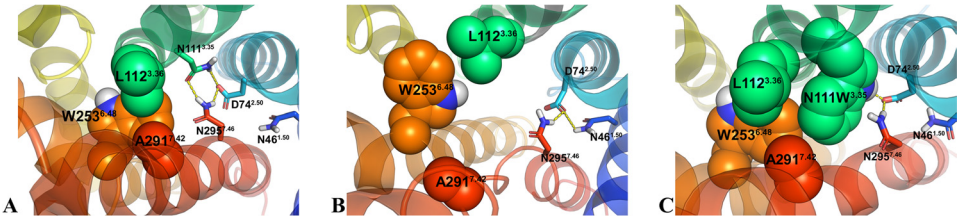


FIGURE 11. **A stable hydrophobic core involving W253$^{6.48}$ is observed in the inactivable N111W-AT$_1$ receptor.** Snapshots of the 84-ns MD simulations show the orientation of the highly conserved W253$^{6.48}$ (*orange spheres*). *A*, in the AT$_1$ receptor, the indole group of W253$^{6.48}$ is oriented toward the hydrophobic core (L112 in *green spheres*; A291 in *red spheres*). *B*, in the N111G-AT$_1$ receptor, the indole group of W253$^{6.48}$ is oriented toward TMD5 (*yellow helix*). *C*, in the N111W-AT$_1$ receptor, the indole group of W253$^{6.48}$ is oriented toward the hydrophobic core (N111W$^{3.35}$ and L112$^{3.36}$ in *green* spheres; A291$^{7.42}$ in *red spheres*).

**TABLE 2**

**Binding properties of $^{125}$I-[Sar$^1$,Ile$^8$]AngII to AT$_1$ receptor mutants**

Cells expressing the indicated receptor were assayed for their binding properties as described under "Experimental Procedures." Binding affinities ($K_d$) and maximal binding capacities ($B_{max}$) were obtained in saturation binding experiments using $^{125}$I-[Sar$^1$,Ile$^8$]AngII. In dose displacement experiments, the tracer $^{125}$I-[Sar$^1$,Ile$^8$]AngII competed with increasing concentrations of AngII, and the IC$_{50}$ values were converted to $K_d$ values using the Cheng-Prusoff equation. All values are expressed as the means ± S.D. of values obtained in *n* independent experiments performed in duplicate.

| Receptor mutant | $K_d$ | | $B_{max}$ | *n* |
|---|---|---|---|---|
| | $^{125}$I-[Sar$^1$,Ile$^8$]AngII | AngII | | |
| | *nM* | | *pmol/mg* | |
| AT$_1$ | 1.9 ± 0.7 | 3.8 ± 0.3 | 1.5 ± 0.2 | 8 |
| N111G-AT$_1$ | 2.7 ± 0.1 | 1.5 ± 0.4 | 0.9 ± 0.1 | 5 |
| N111W-AT$_1$ | 7.7 ± 2.3 | 5.7 ± 1.5 | 0.7 ± 0.1 | 4 |
| N46G-AT$_1$ | 6.4 ± 0.9 | 9.6 ± 2.8 | 1.1 ± 0.1 | 4 |
| N111G/N46G-AT$_1$ | 6.9 ± 2.5 | 6.8 ± 1.5 | 0.7 ± 0.1 | 4 |
| D74N-AT$_1$ | 4.1 ± 1.2 | 4.5 ± 1.3 | 0.4 ± 0.03 | 3 |
| N111G/D74N-AT$_1$ | 4.4 ± 1.0 | 6.4 ± 1.1 | 0.2 ± 0.02 | 3 |
| F77A-AT$_1$ | 4.3 ± 1.4 | 3.2 ± 1.1 | 1.7 ± 0.4 | 5 |
| N111W/F77A-AT$_1$ | 3.1 ± 0.6 | 2.2 ± 0.8 | 1.5 ± 0.2 | 5 |

**TABLE 3**

**Functional properties of mutant AT$_1$ receptors**

HEK293 cells expressing mutant AT$_1$ receptors were assayed for their IP$_1$ production as described under "Experimental Procedures." EC$_{50}$ values are expressed as the means ± S.D. of values obtained in *n* independent experiments performed in duplicate. ND, no detectable response.

| | EC$_{50}$ | *n* |
|---|---|---|
| | *nM* | |
| AT$_1$ | 2.4 ± 1.5 | 12 |
| N111G-AT$_1$ | 3.3 ± 1.1 | 6 |
| N111W-AT$_1$ | ND | 7 |
| N46G-AT$_1$ | 35.8 ± 13.5 | 6 |
| N111G/N46G-AT$_1$ | ND | 6 |
| D74N-AT$_1$ | ND | 5 |
| N111G/D74N-AT$_1$ | ND | 5 |
| F77A-AT$_1$ | 2.1 ± 1.1 | 7 |
| N111W/F77A-AT$_1$ | 3.7 ± 1.8 | 7 |

remained in a *gauche* (−) conformation (Fig. 4*A*). This interaction can be explained by the fact that in the N111W-AT$_1$ receptor, the $\chi_2$ angle of residue N46$^{1.50}$ adopted a *gauche* (+) orientation 51.7% of the time during the MD simulation (Fig. 4*B*), which brings the Nδ2 atom close to the carboxylate of D74$^{1.50}$. Thus, it appears that the mutation of residue N111$^{3.35}$ to a tryptophan stabilizes its interaction with the side chain of residue D74$^{2.50}$ while at the same time allowing the side chain of D74$^{2.50}$ to interact more frequently with the side chain of N46$^{1.50}$ while keeping its $\chi_1$ angle in a *gauche* (−) conformation.

*The N111W Mutation Stabilizes the Hydrophobic Core between TMD3 and TMD7*—MD simulations revealed that both the AT$_1$ receptor and the N111W-AT$_1$ receptor display a similar binding pocket with the hydrophobic core stabilized in a "closed," packed state (Fig. 7*C*). Indeed, the number of water molecules in the vicinity of the hydrophobic core (Fig. 8) and the distance between TMD3 and TMD7 (Fig. 10) in the N111W-AT$_1$ receptor are comparable with those observed in the AT$_1$ receptor. In addition, the highly conserved W253$^{6.48}$, known as the tryptophan toggle switch, adopts a very similar conformation in both the AT$_1$ receptor and the N111W-AT$_1$ receptor. However, in contrast to the AT$_1$ receptor, the introduced aromatic tryptophan residue at position 111$^{3.35}$ of the N111W-AT$_1$ receptor provides additional hydrophobic interaction to the hydrophobic core. Notably, the MD trajectories suggest that residue W111$^{3.35}$ forms π-stacking interactions with residue F77$^{2.53}$, which is also involved in aromatic interactions with Y292$^{7.43}$ (Fig. 13). The indole moiety of W111 apparently stabilizes the hydrophobic cluster involving L112$^{3.36}$, A291$^{7.42}$, and W253$^{6.48}$ at the bottom of the hydrophobic core (Fig. 11*C*). Consequently, the substitution of the asparagine at position 111 for a tryptophan stabilizes the interaction with residue D74$^{2.50}$ and adds favorable hydrophobic interaction to the hydrophobic core. Both effects are consistent with a stabilization of an inactive state.

*The Hydrophobic Core Stabilizes the Inactive Conformation of the Receptor*—To evaluate the contribution of F77$^{2.53}$ to the stability of the hydrophobic core, it was substituted for an alanine, and the functional properties of mutant receptors were evaluated (Table 3). Binding experiments revealed that the mutant receptors were efficiently expressed and exhibited high binding affinities (Table 2). Fig. 12*C* shows that the N111W-AT$_1$ receptor was very poorly activated, producing a maximal level of IP$_1$ (36.5 ± 2.4 nM) severalfold lower than that of the AT$_1$ receptor. The double mutant F77A/N111W-AT$_1$ receptor was much more efficient with a maximal IP$_1$ production of 118.3 ± 5.9 nM, corresponding to 50% of that of the AT$_1$ receptor. Moreover, the basal (45.9 ± 6.6 nM) and AngII-induced (281.6 ± 8.4 nM) activities of the single mutant F77A-AT$_1$

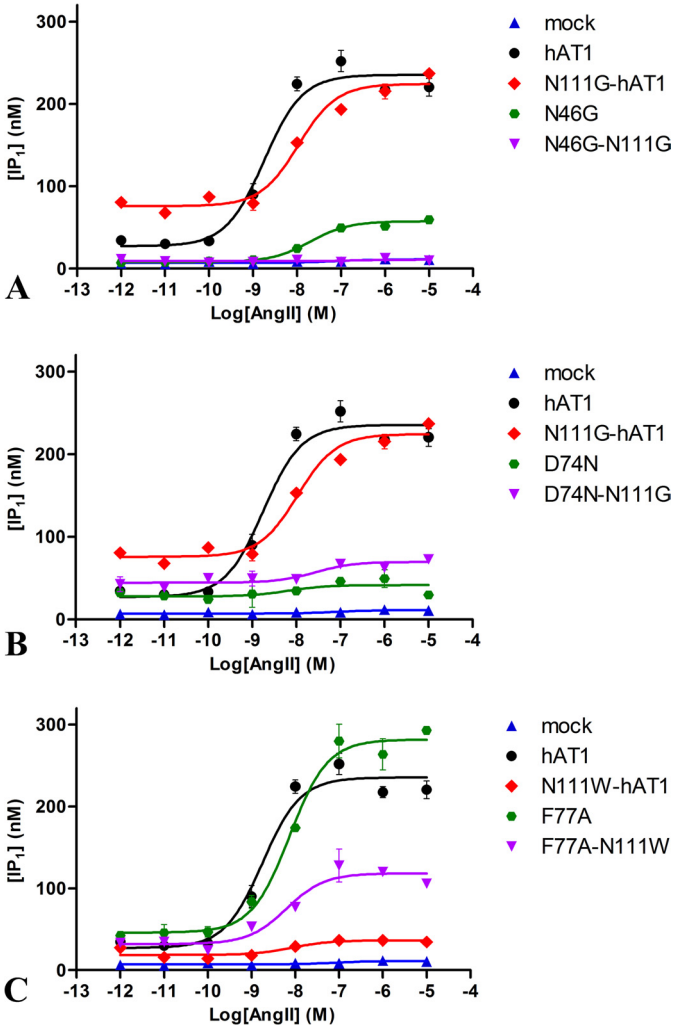


FIGURE 12. **Dose-response curve of IP$_1$ production for AT$_1$ receptor mutants.** HEK293 cells were transfected with the indicated receptor, and their IP$_1$ production was assayed as described under "Experimental Procedures." Each *point* represents the mean of duplicate determinations of a typical experiment, which is representative of at least three independent experiments. *Error bars* represent S.D.

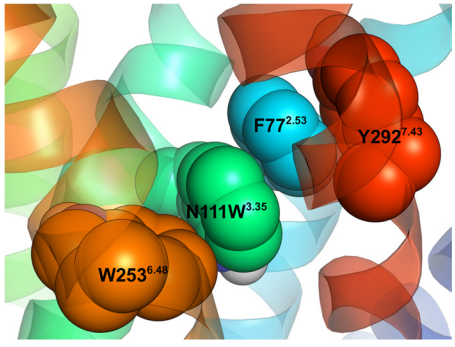


FIGURE 13. **Snapshot of the 84-ns MD simulation of the N111W-AT$_1$ receptor showing the aromatic residues within the hydrophobic core.** Residues N111W$^{3.35}$ (*green*), F77$^{2.53}$ (*blue*),Y292$^{7.43}$ (*red*), and W253$^{6.48}$ (*orange*) are shown.

receptor were both slightly higher than that of the AT$_1$ receptor. These results suggest that weakening the hydrophobic core partially rescues the functional properties of a receptor harboring the N111W mutation. More generally, the results highlight the importance of the hydrophobic core for the stabilization of the inactive state of the AT$_1$ receptor.

## DISCUSSION

Using an approach combining MD simulations and structure-function relationships, we have unveiled a molecular mechanism that could explain the constitutive activity of the N111G-AT$_1$ receptor and the inactivity of the N111W-AT$_1$ receptor. MD simulations suggested that the N111G mutation leads to the disruption of an H-bond network observed in the homology model of the AT$_1$ receptor, presumably in its inactive form. This H-bond network involves the stabilization of the D74$^{2.50}$ side chain by the side chains of residues N111$^{3.35}$ and N295$^{7.46}$ (the N111-D74-N295 network). On the other hand, the N111G mutation leads to the formation of a new H-bond network where the side chain of D74$^{2.50}$ interacts with the side chains of N295$^{7.46}$ and N46$^{1.50}$ (the N46-D74-N295 network). These results suggest that the reorientation of D74$^{2.50}$ from N111$^{3.35}$ to N46$^{1.50}$ is a molecular switch involved in the constitutive activation of the receptor. The substitution of N46 for a glycine abolished the constitutive activity and strongly reduced the agonist-induced activation, supporting the importance of N46$^{1.50}$ in the constitutive and agonist-induced activity of the AT$_1$ receptor. A MD simulation approach using bacteriorhodopsin as template previously proposed that in the inactive conformation of AT$_1$ receptor the residue N111$^{3.35}$ forms an H-bond with residue Y292$^{7.43}$ (65). In our model using CXCR4 receptor as template, this interaction was never observed. Indeed, our model suggests that Y292$^{7.43}$ and N111$^{3.35}$ are too distant to form an H-bond. In our MD simulations, residue Y292$^{7.43}$ points upward toward the extracellular side as $\chi_1$ is maintained in a *gauche* (−) conformation in all three simulations. With $\chi_1$ in a *trans* or *gauche* (+) conformation, the side chain of Y292$^{7.43}$ would clash with the backbone of TMD1 or TMD7, respectively, except in the N111G-AT$_1$ receptor where TMD7 is locally distorted. In that case, Y292$^{7.43}$ could potentially interact with D74$^{2.50}$ if it were to adopt a *trans* conformation.

MD simulations of the N111W-AT$_1$ receptor suggested that tryptophan111 stabilizes the W111-D74-N295 network and the hydrophobic core involving residues F77, V108, L112, W253, I288, A291, and F292. We propose that these are the basis for stabilizing the inactive state of the N111W-AT$_1$ receptor. In support of this assertion, the substitution of residue F77$^{2.53}$ for an alanine provided some agonist-induced activity to the double mutant F77A-N111W-AT$_1$ receptor, thus partially rescuing the inactivity conferred by the N111W mutation. Interestingly, this hydrophobic cluster is unstable and opened during the MD simulation of the constitutively active N111G-AT$_1$ receptor. These results suggest that the N111$^{3.35}$-D74$^{2.50}$-N295$^{7.46}$ H-bond network and the hydrophobic core act in concert to stabilize the inactive state of the AT$_1$ receptor. The results reported here were obtained from a limited simulation time (84 ns) and in that regard furnish information exclusively on the local effects of the mutations. Much longer simulations are needed to evaluate the consequences of the changes in the H-bond network and hydrophobic core on the transmission of the information across the whole receptor and to the cytosolic

domains engaging the interaction with the G protein and other effectors.

The results obtained with the MD simulations are consistent with the results obtained in previous experiments using the substituted cysteine accessibility method to probe for differences in the solvent accessibility of residues delimiting the binding pocket of the $AT_1$ that have shown that residue $A291^{7.42}$ becomes more accessible to the solvent (18). Furthermore, photolabeling experiments have shown that position 77 was more accessible to a photoreactive AngII analog in the N111G-$AT_1$ receptor than in the wild type $AT_1$ receptor (12, 13). These experiments also showed that TMD7 in both the $AT_1$ receptor and the N111G-$AT_1$ receptor could be photolabeled by the antagonist [$Sar^1$,$Bpa^8$]AngII from residues $293^{7.43}$ through $297^{7.48}$. This supports our results from the MD simulation of the N111G-$AT_1$ receptor suggesting that TMD7 can be locally distorted. Moreover, the N111G-$AT_1$ receptor is more permissive than the $AT_1$ receptor to accommodate AngII analogs with bulky modifications (66). These results suggest that the region of the receptor encompassing the hydrophobic core is opened and becomes part of the ligand binding pocket when the hydrophobic core is disrupted. Oliveira *et al.* (67) proposed a similar mechanism involving the expansion of the seven-transmembrane bundle upon activation of bovine rhodopsin and the $AT_1$ receptor. Our results suggest that this expansion through the disruption of the hydrophobic core has an impact on the orientation of residue $W253^{6.48}$. The reorientation of the conserved $W253^{6.48}$, known as the "tryptophan toggle switch" has been suggested to be a crucial part of the activation mechanism of several GPCRs (7, 8, 64, 68, 69). However, recent crystal structures of the $\beta_1$-adrenergic receptor and $\beta_2$-adrenergic receptor with a bound agonist as well as of a photoactivated constitutively active mutant of rhodopsin feature this tryptophan side chain in the same rotamer as their "inactive" counterpart (70–73). This indicates that the conformation of this side chain is not the sole determinant for activation. In accordance, we observed in our simulations with the $AT_1$ receptor that the indole moiety of $W^{6.48}$ packed between small hydrophobic residues at position 7.42 ($A291^{7.42}$) and 3.36 ($L112^{3.36}$). Hence, the reorientation appeared to be the result of an increased hydration of the ligand binding pocket caused by the N111G mutation, resulting in an unfavorable environment for the hydrophobic portion of the indole moiety. A similar event could occur in other GPCRs and promote a movement of $W^{6.48}$ while not causing it to be stabilized in a different rotamer. We therefore suggest that the disruption of the hydrophobic core within the N111G-$AT_1$ receptor influences the conformation and the mobility of the tryptophan toggle switch. Notably, a recent study suggests that $W^{6.48}$ in the human CXCR1 receptor may adopt many different configurations (74).

The mechanisms of stabilization of the inactive state unveiled here might shed light on previous studies performed on the $AT_1$ receptor. Notably, it was suggested that only the size of residue $N111^{3.35}$ was responsible for its role as a conformational switch, not its polarity or potential to form H-bonds (26). Our results actually suggest that both properties can have an impact on the stabilization of the inactive state as position $111^{3.35}$ can stabilize the inactive state either via its polar interaction with $D74^{2.50}$ or by contacting the hydrophobic core.

Interestingly, an interaction between residues $N^{3.35}$ and $D^{2.50}$ is present in the crystal structures of the CXCR4 (14) and the opioid receptors (2–5). Moreover, the crystal structures of the opioid receptors show an interaction between $D^{2.50}$ and $S^{7.46}$. As such, the three residues corresponding to the $N111^{3.35}$-$D74^{2.50}$-$N295^{7.46}$ network within the $AT_1$ receptor form a similar H-bond network in the crystal structures of the opioid receptors. Whether this H-bond network is involved in the activation of opioid receptors is still an open question. However, considering that the $\mu$-, $\kappa$-, and $\delta$-opioid receptors possess some constitutive activity (75) and knowing that the substitution of residue $N295^{7.46}$ for a serine produces a pseudo-constitutively active $AT_1$ receptor (16, 76), it is tempting to suggest that it is. Moreover, the recently released structure of the CXCR1 receptor suggests that in its active state an H-bond is formed between the side chains of residues $N57^{1.50}$ and $D85^{2.50}$ (74). This H-bond is analogous to the $N46^{1.50}$-$D74^{2.50}$ H-bond observed in the N111G-$AT_1$ receptor.

Previous work by Balmforth *et al.* (76) proposed that the side chains of $N111^{3.35}$ and $N295^{7.46}$ would form an H-bond in the inactive conformation of the $AT_1$ receptor and that it would be broken during activation, which are coherent with the results from our simulations. Furthermore, Perlman *et al.* (77) suggested that the formation of an H-bond between the side chains of $D71^{2.50}$ and $N43^{1.50}$ was necessary for the activation of the thyrotropin-releasing hormone receptor. MD simulations of this receptor featured a local perturbation of the helicity of TMD7 as observed in MD simulation of the N111G-$AT_1$ receptor. Interestingly, mutation N43A considerably hampered the activation of the thyrotropin-releasing hormone receptor, implying a similar role for residue $N^{1.50}$ in both the $AT_1$ receptor and the thyrotropin-releasing hormone receptor. However, the role played by this highly conserved $N^{1.50}$ in the activation mechanism of the $AT_1$ receptor appears to be different from its role in the activation mechanism of the $\beta_2$-adrenergic receptor. Indeed, the loss of the polar side chain decreased the constitutive and the agonist-induced activity of the $AT_1$ receptor, whereas it did the opposite to the $\beta_2$-adrenergic receptor (24). Furthermore, the MD simulations suggested direct side chain-side chain interactions between residues $D74^{2.50}$-$N295^{7.46}$ and $D74^{2.50}$-$N46^{1.50}$ in the $AT_1$ receptor, whereas the corresponding interactions are water-mediated in the $\beta_2$-adrenergic receptor (24). Thus, depending on the receptor, the conserved polar residues forming the H-bond networks can act in different ways and through different means.

In conclusion, MD simulations using homology models and structure-function relationships revealed key interactions associated with the activation of the $AT_1$ receptor and with the stabilization of its inactive state. The H-bond network involving $N111^{3.35}$, $D74^{2.50}$, and $N295^{7.46}$ is associated with the inactive state, whereas the H-bond network involving $D74^{2.50}$, $N46^{1.50}$, and $N295^{7.46}$ is associated with the activation of the $AT_1$ receptor. Furthermore, the stabilization of a hydrophobic cluster above the N111-D74-N295 H-bond network is associated with the stabilization of the inactive state of the receptor. These results highlight the importance of the formation of an H-bond

between residues D74 and N46 in the activation process of the $AT_1$ receptor.

## REFERENCES


1. Katritch, V., Cherezov, V., and Stevens, R. C. (2012) Diversity and modularity of G protein-coupled receptor structures. *Trends Pharmacol. Sci.* **33,** 17–27
2. Manglik, A., Kruse, A. C., Kobilka, T. S., Thian, F. S., Mathiesen, J. M., Sunahara, R. K., Pardo, L., Weis, W. I., Kobilka, B. K., and Granier, S. (2012) Crystal structure of the $\mu$-opioid receptor bound to a morphinan antagonist. *Nature* **485,** 321–326
3. Wu, H., Wacker, D., Mileni, M., Katritch, V., Han, G. W., Vardy, E., Liu, W., Thompson, A. A., Huang, X. P., Carroll, F. I., Mascarella, S. W., Westkaemper, R. B., Mosier, P. D., Roth, B. L., Cherezov, V., and Stevens, R.C. (2012) Structure of the human $\kappa$-opioid receptor in complex with JDTic. *Nature* **485,** 327–332
4. Thompson, A. A., Liu, W., Chun, E., Katritch, V., Wu, H., Vardy, E., Huang, X. P., Trapella, C., Guerrini, R., Calo, G., Roth, B. L., Cherezov, V., and Stevens, R. C. (2012) Structure of the nociceptin/orphanin FQ receptor in complex with a peptide mimetic. *Nature* **485,** 395–399
5. Granier, S., Manglik, A., Kruse, A. C., Kobilka, T. S., Thian, F. S., Weis, W. I., and Kobilka, B. K. (2012) Structure of the $\delta$-opioid receptor bound to naltrindole. *Nature* **485,** 400–404
6. Worth, C. L., Kleinau, G., and Krause, G. (2009) Comparative sequence and structural analyses of G-protein-coupled receptor crystal structures and implications for molecular models. *PLoS One* **4,** e7011
7. Schwartz, T. W., Frimurer, T. M., Holst, B., Rosenkilde, M. M., and Elling, C. E. (2006) Molecular mechanism of 7TM receptor activation—a global toggle switch model. *Annu. Rev. Pharmacol. Toxicol.* **46,** 481–519
8. Holst, B., Nygaard, R., Valentin-Hansen, L., Bach, A., Engelstoft, M. S., Petersen, P. S., Frimurer, T. M., and Schwartz, T. W. (2010) A conserved aromatic lock for the tryptophan rotameric switch in TM-VI of seven-transmembrane receptors. *J. Biol. Chem.* **285,** 3973–3985
9. Lebon, G., Warne, T., Edwards, P. C., Bennett, K., Langmead, C. J., Leslie, A. G., and Tate, C. G. (2011) Agonist-bound adenosine A2A receptor structures reveal common features of GPCR activation. *Nature* **474,** 521–525
10. de Gasparo, M., Catt, K. J., Inagami, T., Wright, J. W., and Unger, T. (2000) International Union of Pharmacology. XXIII. The angiotensin II receptors. *Pharmacol. Rev.* **52,** 415–472
11. Auger-Messier, M., Clement, M., Lanctot, P. M., Leclerc, P. C., Leduc, R., Escher, E., and Guillemette, G. (2003) The constitutively active N111G-AT1 receptor for angiotensin II maintains a high affinity conformation despite being uncoupled from its cognate G protein Gq/11$\alpha$. *Endocrinology* **144,** 5277–5284
12. Arsenault, J., Cabana, J., Fillion, D., Leduc, R., Guillemette, G., Lavigne, P., and Escher, E. (2010) Temperature dependent photolabeling of the human angiotensin II type 1 receptor reveals insights into its conformational landscape and its activation mechanism. *Biochem. Pharmacol.* **80,** 990–999
13. Clément, M., Cabana, J., Holleran, B. J., Leduc, R., Guillemette, G., Lavigne, P., and Escher, E. (2009) Activation induces structural changes in the liganded angiotensin II type 1 receptor. *J. Biol. Chem.* **284,** 26603–26612
14. Wu, B., Chien, E. Y., Mol, C. D., Fenalti, G., Liu, W., Katritch, V., Abagyan, R., Brooun, A., Wells, P., Bi, F. C., Hamel, D. J., Kuhn, P., Handel, T. M., Cherezov, V., and Stevens, R.C. (2010) Structures of the CXCR4 chemokine GPCR with small-molecule and cyclic peptide antagonists. *Science* **330,** 1066–1071
15. Bihoreau, C., Monnot, C., Davies, E., Teutsch, B., Bernstein, K. E., Corvol, P., and Clauser, E. (1993) Mutation of Asp74 of the rat angiotensin II receptor confers changes in antagonist affinities and abolishes G-protein coupling. *Proc. Natl. Acad. Sci. U.S.A.* **90,** 5133–5137
16. Feng, Y. H., Zhou, L., Qiu, R., and Zeng, R. (2005) Single mutations at Asn295 and Leu305 in the cytoplasmic half of transmembrane $\alpha$-helix domain 7 of the AT1 receptor induce promiscuous agonist specificity for angiotensin II fragments: a pseudo-constitutive activity. *Mol. Pharmacol.* **68,** 347–355
17. Pérodin, J., Deraët, M., Auger-Messier, M., Boucard, A. A., Rihakova, L., Beaulieu, M. E., Lavigne, P., Parent, J. L., Guillemette, G., Leduc, R., and Escher, E. (2002) Residues 293 and 294 are ligand contact points of the human angiotensin type 1 receptor. *Biochemistry* **41,** 14348–14356
18. Boucard, A. A., Roy, M., Beaulieu, M. E., Lavigne, P., Escher, E., Guillemette, G., and Leduc, R. (2003) Constitutive activation of the angiotensin II type 1 receptor alters the spatial proximity of transmembrane 7 to the ligand-binding pocket. *J. Biol. Chem.* **278,** 36628–36636
19. Martin, S. S., Boucard, A. A., Clément, M., Escher, E., Leduc, R., and Guillemette, G. (2004) Analysis of the third transmembrane domain of the human type 1 angiotensin II receptor by cysteine scanning mutagenesis. *J. Biol. Chem.* **279,** 51415–51423
20. Clément, M., Martin, S. S., Beaulieu, M. E., Chamberland, C., Lavigne, P., Leduc, R., Guillemette, G., and Escher, E. (2005) Determining the environment of the ligand binding pocket of the human angiotensin II type I (hAT1) receptor using the methionine proximity assay. *J. Biol. Chem.* **280,** 27121–27129
21. Martin, S. S., Holleran, B. J., Escher, E., Guillemette, G., and Leduc, R. (2007) Activation of the angiotensin II type 1 receptor leads to movement of the sixth transmembrane domain: analysis by the substituted cysteine accessibility method. *Mol. Pharmacol.* **72,** 182–190
22. Domazet, I., Holleran, B. J., Martin, S. S., Lavigne, P., Leduc, R., Escher, E., and Guillemette, G. (2009) The second transmembrane domain of the human type 1 angiotensin II receptor participates in the formation of the ligand binding pocket and undergoes integral pivoting movement during the process of receptor activation. *J. Biol. Chem.* **284,** 11922–11929
23. Domazet, I., Martin, S. S., Holleran, B. J., Morin, M. E., Lacasse, P., Lavigne, P., Escher, E., Leduc, R., and Guillemette, G. (2009) The fifth transmembrane domain of angiotensin II Type 1 receptor participates in the formation of the ligand-binding pocket and undergoes a counterclockwise rotation upon receptor activation. *J. Biol. Chem.* **284,** 31953–31961
24. Nygaard, R., Valentin-Hansen, L., Mokrosinski, J., Frimurer, T. M., and Schwartz, T. W. (2010) Conserved water-mediated hydrogen bond network between TM-I, -II, -VI, and -VII in 7TM receptor activation. *J. Biol. Chem.* **285,** 19625–19636
25. Noda, K., Feng, Y. H., Liu, X. P., Saad, Y., Husain, A., and Karnik, S. S. (1996) The active state of the AT1 angiotensin receptor is generated by angiotensin II induction. *Biochemistry* **35,** 16435–16442
26. Feng, Y. H., Miura, S., Husain, A., and Karnik, S. S. (1998) Mechanism of constitutive activation of the AT1 receptor: influence of the size of the agonist switch binding residue $Asn^{111}$. *Biochemistry* **37,** 15791–15798
27. Thomas, W. G., Qian, H., Chang, C. S., and Karnik, S. (2000) Agonist-induced phosphorylation of the angiotensin II ($AT_{1A}$) receptor requires generation of a conformation that is distinct from the inositol phosphate-signaling state. *J. Biol. Chem.* **275,** 2893–2900
28. Le, M. T., Vanderheyden, P. M., Szaszák, M., Hunyady, L., and Vauquelin, G. (2002) Angiotensin IV is a potent agonist for constitutive active human AT1 receptors. Distinct roles of the N- and C-terminal residues of angiotensin II during AT1 receptor activation. *J. Biol. Chem.* **277,** 23107–23110
29. Miura, S., Zhang, J., Boros, J., and Karnik, S. S. (2003) TM2-TM7 interaction in coupling movement of transmembrane helices to activation of the angiotensin II type-1 receptor. *J. Biol. Chem.* **278,** 3720–3725
30. Nikiforovich, G. V., Mihalik, B., Catt, K. J., and Marshall, G. R. (2005) Molecular mechanisms of constitutive activity: mutations at position 111 of the angiotensin AT1 receptor. *J Pept. Res.* **66,** 236–248
31. Lee, C., Hwang, S. A., Jang, S. H., Chung, H. S., Bhat, M. B., and Karnik, S. S. (2007) Manifold active-state conformations in GPCRs: agonist-activated constitutively active mutant AT1 receptor preferentially couples to Gq compared to the wild-type AT1 receptor. *FEBS Lett.* **581,** 2517–2522
32. Miura, S., Kiya, Y., Kanazawa, T., Imaizumi, S., Fujino, M., Matsuo, Y., Karnik, S. S., and Saku, K. (2008) Differential bonding interactions of inverse agonists of angiotensin II type 1 receptor in stabilizing the inactive state. *Mol. Endocrinol.* **22,** 139–146
33. Bhuiyan, M. A., Hossain, M., Miura, S., Nakamura, T., Ozaki, M., and Nagatomo, T. (2009) Constitutively active mutant N111G of angiotensin II type 1 ($AT_1$) receptor induces homologous internalization through mediation of $AT_1$-receptor antagonist. *J. Pharmacol. Sci.* **111,** 227–234
34. Bhuiyan, M. A., Hossain, M., Nakamura, T., Ozaki, M., and Nagatomo, T.

(2010) Internalization of constitutively active N111G MUTANT of AT1 receptor induced by angiotensin II-receptor antagonists candesartan, losartan, and telmisartan: comparison with valsartan. *J. Pharmacol. Sci.* **112,** 459–462
35. Yan, L., Holleran, B. J., Lavigne, P., Escher, E., Guillemette, G., and Leduc, R. (2010) Analysis of transmembrane domains 1 and 4 of the human angiotensin II AT1 receptor by cysteine-scanning mutagenesis. *J. Biol. Chem.* **285,** 2284–2293
36. Guillemette, G., and Escher, E. (1983) Analysis of the adrenal angiotensin II receptor with the photoaffinity labeling method. *Biochemistry* **22,** 5591–5596
37. Ballesteros, J. A., and Weinstein, H. (1995) in *Methods in Neurosciences* (Sealfon, S. C., ed) Vol. 25, pp. 366–428, Academic Press, Waltham, MA
38. Zhang, Y. (2007) Template-based modeling and free modeling by I-TASSER in CASP7. *Proteins* **69,** Suppl. 8, 108–117
39. Roy, A., Kucukural, A., and Zhang, Y. (2010) I-TASSER: a unified platform for automated protein structure and function prediction. *Nat. Protoc.* **5,** 725–738
40. Laskowski, R. A., Rullmannn, J. A., MacArthur, M. W., Kaptein, R., and Thornton, J. M. (1996) AQUA and PROCHECK-NMR: programs for checking the quality of protein structures solved by NMR. *J. Biomol. NMR* **8,** 477–486
41. Berendsen, H. J. C., van der Spoel, D., and van Drunen, R. (1995) GROMACS: a message-passing parallel molecular dynamics implementation. *Comput. Phys. Commun.* **91,** 43–56
42. Van Der Spoel, D., Lindahl, E., Hess, B., Groenhof, G., Mark, A. E., and Berendsen, H. J. (2005) GROMACS: fast, flexible, and free. *J. Comput. Chem.* **26,** 1701–1718
43. Hess, B., Kutzner, C., van der Spoel, D., and Lindahl, E. (2008) GROMACS 4: algorithms for highly efficient, load-balanced, and scalable molecular simulation. *J. Chem. Theory Comput.* **4,** 435–447
44. van der Spoel, D., and Hess, B. (2011) GROMACS—the road ahead. *WIREs Comput. Mol. Sci.* **1,** 710–715
45. Kandt, C., Ash, W. L., and Tieleman, D. P. (2007) Setting up and running molecular dynamics simulations of membrane proteins. *Methods* **41,** 475–488
46. Lemkul, J. A., and Bevan, D. R. (2009) Perturbation of membranes by the amyloid $\beta$-peptide: a molecular dynamics study. *FEBS J.* **276,** 3060–3075
47. de Vries, A. H., Mark, A. E., and Marrink, S. J. (2004) The binary mixing behavior of phospholipids in a bilayer: a molecular dynamics study. *J. Phys. Chem. B* **108,** 2454–2463
48. Lemkul, J. A., and Bevan, D. R. (2008) A comparative molecular dynamics analysis of the amyloid $\beta$-peptide in a lipid bilayer. *Arch. Biochem. Biophys.* **470,** 54–63
49. Berweger, C. D., van Gunsteren, W. F., and Müller-Plathe, F. (1995) Force field parametrization by weak coupling. Re-engineering SPC water. *Chem. Phys. Lett.* **232,** 429–436
50. Berger, O., Edholm, O., and Jähnig, F. (1997) Molecular dynamics simulations of a fluid bilayer of dipalmitoylphosphatidylcholine at full hydration, constant pressure, and constant temperature. *Biophys. J.* **72,** 2002–2013
51. Tieleman, D. P. (2004) The molecular basis of electroporation. *BMC Biochem.* **5,** 10
52. Tieleman, D. P., Leontiadou, H., Mark, A. E., and Marrink, S. (2003) Simulation of pore formation in lipid bilayers by mechanical stress and electric fields. *J. Am. Chem. Soc.* **125,** 6382–6383
53. MacCallum, J. L., and Tieleman, D. P. (2006) Computer simulation of the distribution of hexane in a lipid bilayer: spatially resolved free energy, entropy, and enthalpy profiles. *J. Am. Chem. Soc.* **128,** 125–130
54. Anézo, C., de Vries, A. H., Höltje, H., Tieleman, D. P., and Marrink, S. (2003) Methodological issues in lipid bilayer simulations. *J. Phys. Chem. B* **107,** 9424–9433
55. Werner, T., Morris, M. B., Dastmalchi, S., and Church, W. B. (2012) Structural modelling and dynamics of proteins for insights into drug interactions. *Adv. Drug Deliv. Rev.* **64,** 323–343
56. Nose, S. (1984) A unified formulation of the constant temperature molecular dynamics methods. *J. Chem. Phys.* **81,** 511–519
57. Hoover, W. G. (1985) Canonical dynamics: equilibrium phase-space distributions. *Phys. Rev. A* **31,** 1695–1697
58. DeLano, W. L. (2010) *The PyMOL Molecular Graphics System*, version 1.3r1, Schrödinger, LLC, New York
59. Corpet, F. (1988) Multiple sequence alignment with hierarchical clustering. *Nucleic Acids Res.* **16,** 10881–10890
60. Ehrhardt, C., Schmolke, M., Matzke, A., Knoblauch, A., Will, C., Wixler, V., and Ludwig, S. (2006) Polyethylenimine, a cost-effective transfection reagent. *Signal Transduct.* **6,** 179–184
61. Cheng, Y., and Prusoff, W. H. (1973) Relationship between the inhibition constant (K1) and the concentration of inhibitor which causes 50 per cent inhibition (I50) of an enzymatic reaction. *Biochem. Pharmacol.* **22,** 3099–3108
62. Kulińska, K., Kuliński, T., Lyubartsev, A., Laaksonen, A., and Adamiak, R. W. (2000) Spatial distribution functions as a tool in the analysis of ribonucleic acids hydration—molecular dynamics studies. *Comput. Chem.* **24,** 451–457
63. Bhattacharya, S., Hall, S. E., Li, H., and Vaidehi, N. (2008) Ligand-stabilized conformational states of human $\beta_2$ adrenergic receptor: insight into G-protein-coupled receptor activation. *Biophys. J.* **94,** 2027–2042
64. Nygaard, R., Frimurer, T. M., Holst, B., Rosenkilde, M. M., and Schwartz, T. W. (2009) Ligand binding and micro-switches in 7TM receptor structures. *Trends Pharmacol. Sci.* **30,** 249–259
65. Joseph, M.-P., Maigret, B., Bonnafous, J.-C., Marie, J., and Scheraga, H. A. (1995) A computer modeling postulated mechanism for angiotensin II receptor activation. *J. Protein Chem.* **14,** 381–398
66. Fillion, D., Lemieux, G., Basambombo, L. L., Lavigne, P., Guillemette, G., Leduc, R., and Escher, E. (2010) The amino-terminus of angiotensin II contacts several ectodomains of the angiotensin II receptor AT1. *J. Med. Chem.* **53,** 2063–2075
67. Oliveira, L., Costa-Neto, C. M., Nakaie, C. R., Schreier, S., Shimuta, S. I., and Paiva, A. C. (2007) The angiotensin II AT1 receptor structure-activity correlations in the light of rhodopsin structure. *Physiol. Rev.* **87,** 565–592
68. Ahuja, S., and Smith, S. O. (2009) Multiple switches in G protein-coupled receptor activation. *Trends Pharmacol. Sci.* **30,** 494–502
69. Colson, A. O., Perlman, J. H., Jinsi-Parimoo, A., Nussenzveig, D. R., Osman, R., and Gershengorn, M. C. (1998) A hydrophobic cluster between transmembrane helices 5 and 6 constrains the thyrotropin-releasing hormone receptor in an inactive conformation. *Mol. Pharmacol.* **54,** 968–978
70. Warne, T., Edwards, P. C., Leslie, A. G., and Tate, C. G. (2012) Crystal structures of a stabilized $\beta$1-adrenoceptor bound to the biased agonists bucindolol and carvedilol. *Structure* **20,** 841–849
71. Deupi, X., Edwards, P., Singhal, A., Nickle, B., Oprian, D., Schertler, G., and Standfuss, J. (2012) Stabilized G protein binding site in the structure of constitutively active metarhodopsin-II. *Proc. Natl. Acad. Sci. U.S.A.* **109,** 119–124
72. Standfuss, J., Edwards, P. C., D'Antona, A., Fransen, M., Xie, G., Oprian, D. D., and Schertler, G. F. (2011) The structural basis of agonist-induced activation in constitutively active rhodopsin. *Nature* **471,** 656–660
73. Rasmussen, S. G., DeVree, B. T., Zou, Y., Kruse, A. C., Chung, K. Y., Kobilka, T. S., Thian, F. S., Chae, P. S., Pardon, E., Calinski, D., Mathiesen, J. M., Shah, S. T., Lyons, J. A., Caffrey, M., Gellman, S. H., Steyaert, J., Skiniotis, G., Weis, W. I., Sunahara, R. K., and Kobilka, B. K. (2011) Crystal structure of the $\beta$2-adrenergic receptor-Gs protein complex. *Nature* **477,** 549–555
74. Park, S. H., Das, B. B., Casagrande, F., Tian, Y., Nothnagel, H. J., Chu, M., Kiefer, H., Maier, K., De Angelis, A. A., Marassi, F. M., and Opella, S. J. (2012) Structure of the chemokine receptor CXCR1 in phospholipid bilayers. *Nature* **491,** 779–783
75. Sadée, W., Wang, D., and Bilsky, E. J. (2005) Basal opioid receptor activity, neutral antagonists, and therapeutic opportunities. *Life Sci.* **76,** 1427–1437
76. Balmforth, A. J., Lee, A. J., Warburton, P., Donnelly, D., and Ball, S. G. (1997) The conformational change responsible for AT1 receptor activation is dependent upon two juxtaposed asparagine residues on transmembrane helices III and VII. *J. Biol. Chem.* **272,** 4245–4251
77. Perlman, J. H., Colson, A. O., Wang, W., Bence, K., Osman, R., and Gershengorn, M. C. (1997) Interactions between conserved residues in transmembrane helices 1, 2, and 7 of the thyrotropin-releasing hormone receptor. *J. Biol. Chem.* **272,** 11937–11942